WIDE-ANGLE ISAR PASSIVE IMAGING USING SMOOTHED PSEUDO WIGNER-VILLE DISTRIBUTION

Yong Wu and David C. Munson, Jr.

Coordinated Science Lab and Department of Electrical and Computer Engineering,
University of Illinois at Urbana-Champaign, Urbana, IL, 61801
email: yongwu@uiuc.edu, d-munson@uiuc.edu

ABSTRACT

We are investigating passive radar imaging of aircraft using reflected TV signals. UHF-band ISAR imaging requires wide-angle data to produce good cross-range resolution. We show that direct Fourier reconstruction (DFR) causes degradation of the reconstructed image due to aspect-dependent scattering. We find that a Smoothed Pseudo Wigner-Ville distribution (SPWVD) applied in the cross-range direction in place of the Fourier transform can generate a sequence of images, which shows the target reflectivity as a function of aspect angle. Compared to DFR results, these images have higher cross-range resolution. A final image can be synthesized from these images and used for target recognition. XPATCH is used to simulate monostatic data from an aircraft. The proposed SPWVD-based imaging method produces a useful image of the aircraft from this data.

1. INTRODUCTION

We are investigating passive radar imaging of aircraft using reflected TV signals. In related work, Lockheed Martin has developed the $SilentSentry^{TM}$ system which can detect and track targets using reflected radio or TV signals [1]. We are interested in forming images of aircraft from passive data, for the purpose of classification. Conventional X-band ISAR imaging systems operate around 10 GHz and use a small synthetic aperture (e.g. 3 degrees) to collect data. We consider a passive radar system that operates around 600 MHz, which is a far lower frequency than X-band. Therefore, a much wider aperture is needed to provide similar cross-range resolution. In a wide aperture scenario, the target's scattering is aspect-dependent (microwave specular reflection and corner/edge diffraction are all aspect-dependent [2, 3]), which will cause problems in direct Fourier reconstruction (DFR). We show that, for two point targets, the reconstructed image using DFR will be blurred if the scattering changes with aspect. A possible solution is the sub-aperture approach: divide the wide aperture into several smaller sub-apertures and form a sub-image using each sub-aperture. A final image can be synthesized from these sub-images. Obviously, the image resolution will suffer.

Time-Frequency (T-F) transforms have been used in moving target ISAR imaging [4]. Here, we apply a T-F transform in the cross-range direction to replace the Fourier transform, since the scattering changes with aspect angle. In fact, the sub-aperture approach is similar to processing the wide-angle data using the Short Time Fourier Transform (STFT) in the cross-range direction and the Fourier transform in the range direction. We find that, if the Smoothed Pseudo Wigner-Ville distribution (SPWVD) is used in the cross-range direction to replace the Fourier transform, a sequence of images can be obtained that show the reflectivity as a function of aspect angle and have higher cross-range resolution than sub-aperture or STFT approaches. These images can be combined to synthesize one final image, which is closer to the optical appearance of the aircraft and easily recognizable. XPATCH is used to generate monostatic data which is used to test our algorithm. It is demonstrated that the SPWVD-based image formation method is superior to sub-aperture and STFT-based approaches.

2. DFR WITH ASPECT-DEPENDENT SCATTERING

We first consider DFR for the reconstruction of an image from Fourier data collected on polar grid [5, 6]. The Fourier data require interpolation to a rectangular grid followed by a 2D FFT to produce the image.

Consider two point targets at (x_0, y_0) and (x_1, y_1), with

This work is supported by DARPA under the contract number F49620-98-1-0498

reflectivity

$$\begin{aligned} f(x,y) &= f_0(x,y) + f_1(x,y) \\ &= \delta(x-x_0, y-y_0) + \delta(x-x_1, y-y_1). \end{aligned} \quad (1)$$

The Fourier transform is

$$F(u,v) = e^{-j(ux_0+vy_0)} + e^{-j(ux_1+vy_1)}. \quad (2)$$

If the two points' scattering data varies with aspect, then the collected data is this Fourier transform, weighted in the u direction according to aspect dependence. Here, we assume that u is the Fourier coordinate corresponding to cross-range. Furthermore, assume that the aspect-dependent weighting has the form $G(u) = e^{-(u-a)^2}$, where $u = k\theta$, k is a constant, θ is the aspect angle and a/k is the aspect angle having maximum reflection. The weighting function is bell-shaped and is chosen for mathematical tractability. The collected data becomes

$$\tilde{F}(u,v) = e^{-j(ux_0+vy_0)}e^{-(u-a_0)^2} + e^{-j(ux_1+vy_1)}e^{-(u-a_1)^2}. \quad (3)$$

If the bandwidth available is wide and Fourier inversion is used, we get

$$\begin{aligned} \tilde{f}(x,y) &\approx f_0(x,y) *_x [e^{-x^2}e^{ja_0x}] + f_1(x,y) *_x [e^{-x^2}e^{ja_1x}] \\ &= \delta(y-y_0)e^{-(x-x_0)^2}e^{ja_0(x-x_0)} + \\ &\quad \delta(y-y_1)e^{-(x-x_1)^2}e^{ja_1(x-x_1)}. \end{aligned} \quad (4)$$

In the x direction, the δ functions are spread out and the complex multiplier may cause cancelation of the two signals. To see this, suppose $x = x_0$. Then, if the two points are very close, $e^{-(x_0-x_1)^2} \approx 1$, thus

$$\tilde{f}(x_0,y) \approx \delta(y-y_0)[1 + e^{ja_1(x_0-x_1)}]. \quad (5)$$

Now, if $e^{ja_1(x_0-x_1)} = -1$ (which is possible), $\tilde{f}(x_0,y) \approx 0$. More generally,

$$\begin{aligned} \tilde{f}(x,y) &\approx \delta(y-y_0)e^{-(x-x_0)^2}e^{ja_0(x-x_0)} \\ &\quad [1 + e^{j[(a_1-a_0)x+a_0x_0-a_1x_1]}]. \end{aligned} \quad (6)$$

The function $\tilde{f}(x,y_0)$ might become very noisy, since the term $[1 + e^{j[(a_1-a_0)x+a_0x_0-a_1x_1]}]$ might vary from 0 to 2 rapidly. Hence, it may be impossible to even detect the two point-targets, and the resulting image quality may be severely degraded. This analysis can be extended to more point targets for an aircraft scattering-center model, suggesting that DFR applied to wide-angle data may degrade image quality.

3. SUB-APERTURE APPROACH

A wide-angle aperture can be divided into several smaller sub-apertures with the reflectivity assumed constant across each sub-aperture. DFR applied to individual sub-apertures yields a set of images. Since the microwave scattering is highly aspect-dependent, only a subset of scatterers of the target actually 'appear' in each observing sub-aperture. This is different from optical imaging of aircraft [7]. Reconstructed images from several sub-apertures can be combined together to yield one final image which may show more scatterers of the target and may be closer to the optical image.

A suggested algorithm for image synthesis from subapertures is: First normalize each sub-aperture image so that the maximum is 1 and minimum is 0; then rotate these sub-aperture images so that the target has the same orientation in each image; assign to each pixel in the synthesized image the maximum of the corresponding pixel values in the subaperture images.

Symmetry enhancement has been suggested by Steinberg [7] to improve the quality of radar images of aircraft, since aircrafts are symmetric. In our algorithm, the maximum magnitude of the two symmetric pixels of the image is taken as the value for both pixels. This will give a more recognizable image for a human observer.

The disadvantage of the sub-aperture approach is that it is difficult to choose a suitable sub-aperture width: to get good azimuth resolution, the subaperture should be large, but then the reflectivity may change significantly across the sub-aperture and the image will be smeared; if the subaperture is too small, the azimuth resolution will be poor and the image quality will be degraded.

4. IMAGE FORMATION BASED ON STFT AND WVD

As the reflectivity profile of the target changes with aspect angle, the Fourier data collected over a large azimuth interval will be time-varying (here time refers to the aspect). We can apply a Time-Frequency (T-F) transform in the azimuth direction to replace the Fourier transform to produce a sequence of instantaneous images [8]. T-F transforms have been applied to moving target imaging using the range-doppler approach[4].

The Short Time Fourier Transform (STFT) is a simple T-F transform that can be used. In our problem, the STFT is defined as

$$STFT(u,x) = \frac{1}{2\pi}\int_{-\infty}^{\infty} s(\tau)w(\tau-u)e^{jx\tau}d\tau \quad (7)$$

where $s(u)$ is the Fourier data in the cross-range direction and $w(u)$ is a short-time window function. The STFT has

poor cross-range resolution for a narrow window and is similar to sub-aperture processing with the same window width.

The Wigner-Ville Distribution(WVD) has higher time and frequency resolution than the STFT. We define the WVD in our problem as

$$W(u,x) = \frac{1}{2\pi}\int_{-\infty}^{\infty} s(u+\frac{\tau}{2})s^*(u-\frac{\tau}{2})e^{jx\tau}d\tau. \quad (8)$$

The WVD of the sum of two signals is $W(s_1(u)+s_2(u)) = W_{11}(u,x)+W_{22}(u,x)+2Re\{W_{12}(u,x)\}$. The cross-term $W_{12}(u,x)$ can be suppressed by using the Smoothed Pseudo Wigner-Ville distribution (SPWVD) , which is defined as

$$\begin{aligned} SPWVD(u,x) &= \frac{1}{2\pi}\int_{-\infty}^{\infty}\int_{-\infty}^{\infty} q(u-u')h(x-x') \\ &\quad \cdot WVD(u',x')du'dx'. \end{aligned} \quad (9)$$

where $q(\cdot)$ and $h(\cdot)$ are the smoothing window functions (e.g. Hamming windows). The SPWVD allows the smoothing spread in u and x to be adjusted independently of each other. Thus it can have better time-frequency resolution than the STFT, which requires a tradeoff between the spread in u and x [9].

For the two point-target model, we assume aspect weighting functions $G_0(u) = e^{-\frac{(u-a_0)^2}{b_0}}$ and $G_1(u) = e^{-\frac{(u-a_1)^2}{b_1}}$, where b_i indicates the pulse width of each weighting function in the Fourier data. Then the collected data becomes

$$\tilde{F}(u,v) = e^{-j(ux_0+vy_0)}G_0(u) + e^{-j(ux_1+vy_1)}G_1(u). \quad (10)$$

Applying the WVD to the weighted data in the u direction, we get the reconstructed image

$$\begin{aligned} &\tilde{f}(x,y,u) = B\sqrt{2\pi/b_0}sinc[B(y-y_0)](B-2\mid u\mid) \\ &\{sinc[(x-x_0)(B-2\mid u\mid)] *_x e^{-2b_0x^2}\}e^{-\frac{2\pi^2}{b_0}(u-a_0)^2} \\ &+B\sqrt{2\pi/b_1}sinc[B(y-y_1)](B-2\mid u\mid) \\ &\{sinc[(x-x_1)(B-2\mid u\mid)] *_x e^{-2b_1x^2}\}e^{-\frac{2\pi^2}{b_1}(u-a_1)^2} \\ &+crossterms. \end{aligned} \quad (11)$$

where $*_x$ indicates convolution in x, $\mid u \mid \leq B/2$, B is the bandwidth in the cross-range direction. The cross-terms can be suppressed by the SPWVD, which convolves Eq. (11) with the window functions in the u and x directions. Thus a sequence of images is produced for different values of u:

$$f'(x,y,u) = [\tilde{f}(x,y,u) *_u q(u)] *_x h(x). \quad (12)$$

We can model a set of scatterers with aspect-dependent reflectivity as

$$f(x,y,\theta) = \sum_{i=0}^{N} A_i\delta(x-x_i, y-y_i)e^{-\frac{(\theta-\theta_i)^2}{c_i}}. \quad (13)$$

where N is the number of scatterers, c_i indicates the pulse width of the scattering profile in θ and θ_i is the orientation having maximum reflection. The sequence of images produced by the SPWVD (assuming cross-terms have been suppressed) is:

$$\begin{aligned} &f'(x,y,u) = [(\sum_{i=0}^{N} A_iB\sqrt{\frac{2\pi}{b_i}}sinc[B(y-y_i)] \\ &(B-2\mid u\mid)\{sinc[(x-x_i)(B-2\mid u\mid)] \\ &*_x e^{-2b_ix^2}\}e^{-\frac{2\pi^2}{b_i}(u-a_i)^2}) *_u q(u)] *_x h(x) \end{aligned} \quad (14)$$

Here f' is the reconstructed $x-y$ reflectivity as a function of aspect angle ($u = k\theta, a_i = k\theta_i$, k is a constant). Since the SPWVD is real and positive, the aspect-dependence does not produce a complex multiplication term in the result, thus avoiding the cancelation of neighboring points. This also ensures that only the subset of scatterers visible at a certain aspect are shown in the corresponding instantaneous image (properly weighted by the weighting functions $e^{-\frac{2\pi^2}{b_i}(u-a_i)^2}$). Interference between adjacent scatterers is avoided.

The SPWVD suppresses cross-terms in WVD, but the resolution is also reduced. Most of the images from the SPWVD have higher resolution than those produced by the STFT using the same data. (For some images with u closer to $B/2$, resolution in x becomes poor and these images are not used to synthesize the final image.) The final synthesized image can show more clearly the shape and reflectivity of the target. Hence it might be very useful for target recognition purposes. The SPWVD-based image formation algorithm is described by the flow chart in Figure 1. For a very-wide-angle data, this algorithm can be used to process data in several 30^o-wide subapertures (with 50% overlap) and produce several synthesized images, which can be combined into one final image using the image synthesis algorithm.

5. SIMULATIONS USING XPATCH DATA

Testing of our image formation algorithm is simplified by using synthetically generated aircraft signatures. Among the prime tools for doing this, XPATCH loses accuracy below about 1 GHz and the Fast Illinois Solver Code (FISC) is very demanding in terms of both computation and memory. Thus, to assist in our preliminary investigations, we have used XPATCH to generate L-band data at frequencies 1 - 1.5 GHz . We expect that our study based on this data will help in understanding wide-angle ISAR imaging at UHF frequencies (400 MHz - 800 MHz).

We simulated monostatic radar echoes from an X29 air-

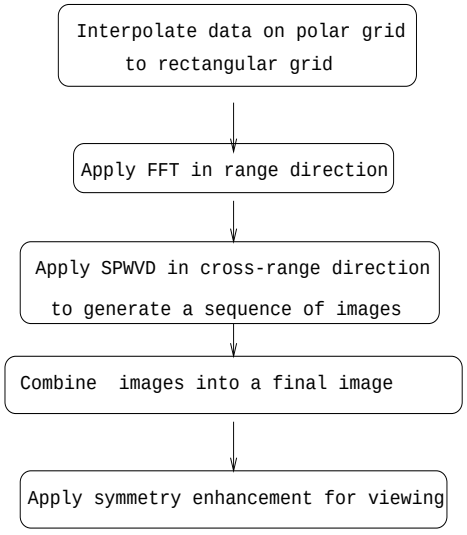

Fig. 1. Flow chart of the SPWVD-based image formation algorithm

craft. The data was simulated from 0^o to 180^o (0^o at nose, 90^o at broadside, and 180^o at tail), 0^o elevation. The frequency step was 6 MHz and the azimuth step was 0.3 degrees. HH polarization was used. Figure 2 shows an optical image of an X29 airplane. Figure 3 shows the log of magnitude of the Fourier data. Figures 4 and 5 show the image formed using all of the data via DFR and the result after symmetry enhancement, which shows only the fuselage (wings are missing). Figures 6, 7 and 8 show the image produced by combining several sub-aperture images from DFR, where each sub-aperture is 60, 15 and 7.5 degrees wide, respectively, with 50 % overlap. The shape of the plane is roughly visible.

Figure 9 shows the result given by STFT processing, which shows more scatterers on the body of the plane, but with even lower resolution. A 3^o wide hamming window was used in the STFT processing. Figure 10 shows the result given by the SPWVD, with better resolution than the previous images. Note that the front part of the aircraft is clearer and the two inlets and the fuselage are shown more clearly in Fig. 10 (they are smeared all together in Figs. 7, 8 and 9). Fig. 6 doesn't show the wings and the front parts of the plane as clearly. All scattering centers are spread out more by the narrow sub-aperture and STFT methods, with the imagery degraded compared to the SPWVD. This suggests that SPWVD-based image formation is superior to the DFR sub-aperture method for aspect-dependent imaging using wide-angle L-band data. We believe that this same observation will hold in the UHF band.

6. CONCLUSION

We studied the wide-angle ISAR passive imaging problem. The DFR method was shown to cause degradation in the reconstructed image for two point targets when the scattering varied with aspect. The sub-aperture approach is less than ideal, since it cannot guarantee good cross-range resolution and small degradation caused by aspect-dependent scattering simultaneously. We showed that, if the SPWVD is used in the cross-range direction to replace the Fourier transform, a sequence of images can be produced which show the reflectivity as a function of aspect. These images have higher quality and better cross-range resolution than those produced by the DFR and sub-aperture methods. They can be combined together to yield one final image, which is closer to the optical image. Simulation results using XPATCH data was given to validate our approach. We expect that the SPWVD-based image formation method might be useful in the UHF-band for ISAR imaging and target classification. The XPATCH data set we used, however, is at a higher frequency and is more complete than could be obtained in a realistic passive scenario. Thus considerable further study is needed.

7. REFERENCES

[1] http://silentsentry.external.lmco.com, "Lockheed Martin web page," .

[2] M. J. Gerry and L. C. Potter, "A parametric model for synthetic aperture radar measurements," *IEEE Trans. Antennas Propagat.*, vol. 47, no. 7, pp. 1179–1188, July 1999.

[3] C. C. Chen and H. C. Andrews, "Multifrequency imaging of radar turntable data," *IEEE Trans. Aerosp. Electron. Syst.*, vol. AES-16, no. 1, pp. 15–22, Jan 1980.

[4] V. C. Chen and S. Qian, "Joint time-frequency transform for radar range-Doppler imaging," *IEEE Trans. Aerosp. Electron. Syst.*, vol. 34, no. 2, pp. 486–499, Apr 1998.

[5] J. L. Walker, "Range-doppler imaging of rotating objects," *IEEE Trans. Aerosp. Electron. Syst.*, vol. AES-16, no. 1, pp. 23–52, Jan 1980.

[6] D. C. Munson Jr., J. D. O'Brien, and W. K. Jenkins, "A tomographic formulation of spotlight mode synthetic aperture radar," *Proc. IEEE*, vol. 71, no. 8, pp. 917–925, Aug 1983.

[7] B. D. Steinberg, "Microwave imaging of aircraft," *Proc. IEEE*, vol. 76, no. 12, pp. 1578–1592, Dec 1988.

[8] L. Cohen, "Time-frequency distributions - a review," *Proc. IEEE*, vol. 77, no. 7, pp. 941–981, Jul 1989.

[9] F. Hlawatsch and G. F. Boudreaux-bartels, "Linear and quadratic time-frequency signal representations," *IEEE SP Magazine*, pp. 21–67, Apr 1992.

Fig. 2. An optical image of an X29 aircraft.

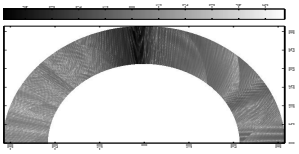

Fig. 3. Log of magnitude of the Fourier data simulated by XPATCH.

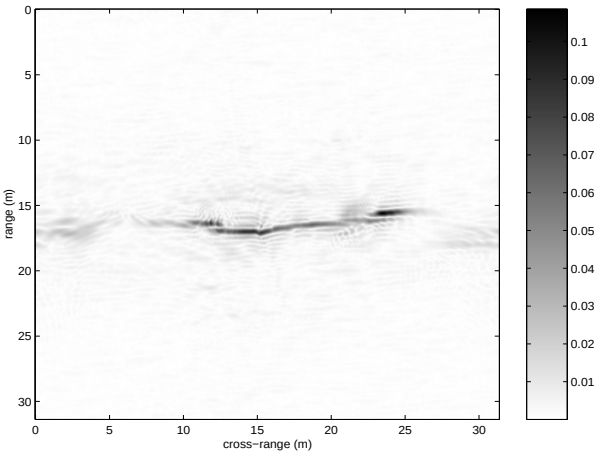

Fig. 4. Image produced by DFR using full-aperture data.

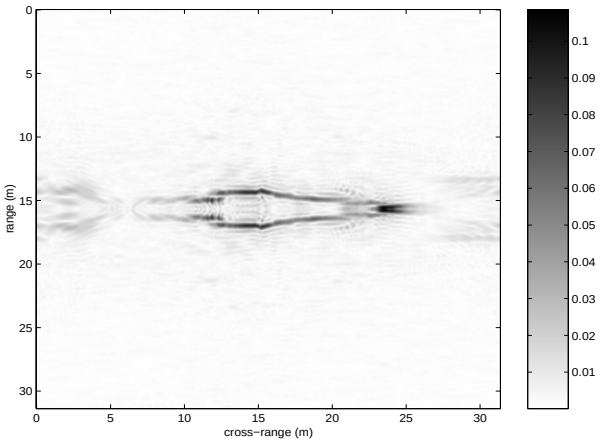

Fig. 5. Image produced by DFR using full-aperture data after symmetry enhancement.

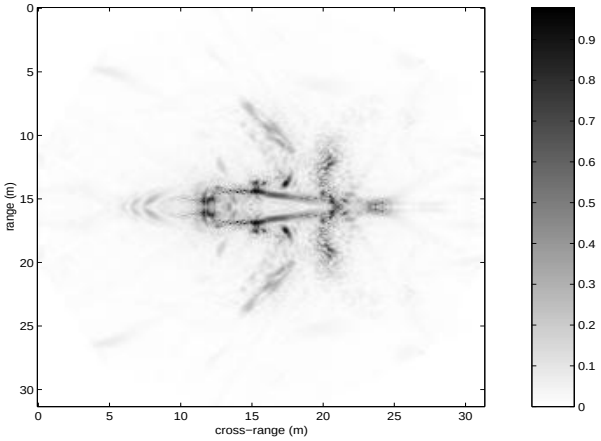

Fig. 6. Synthesized image by DFR from sub-aperture images, each sub-aperture width is 60 degrees.

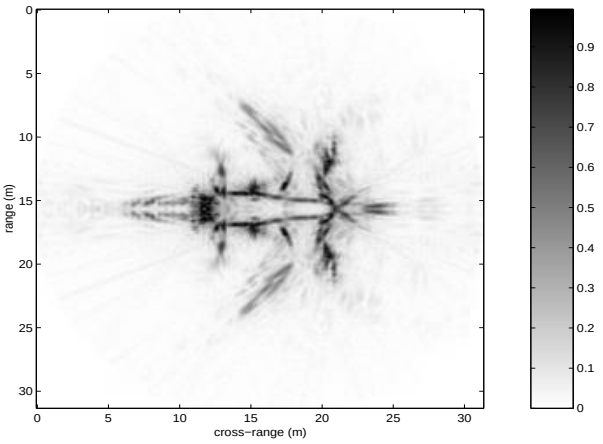

Fig. 7. Synthesized image by DFR from sub-aperture images, each sub-aperture width is 15 degrees.

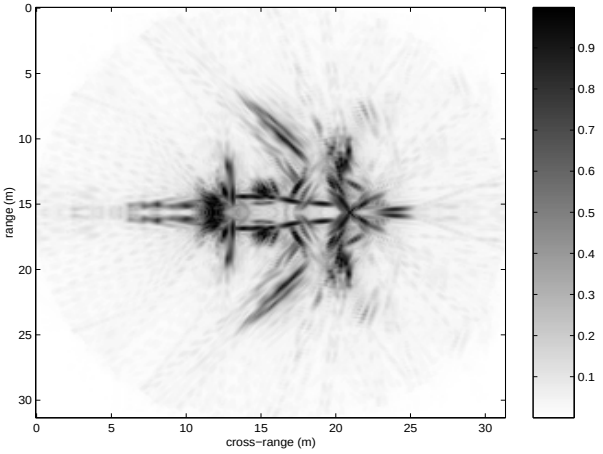

Fig. 8. Synthesized image by DFR from sub-aperture images, each sub-aperture width is 7 degrees.

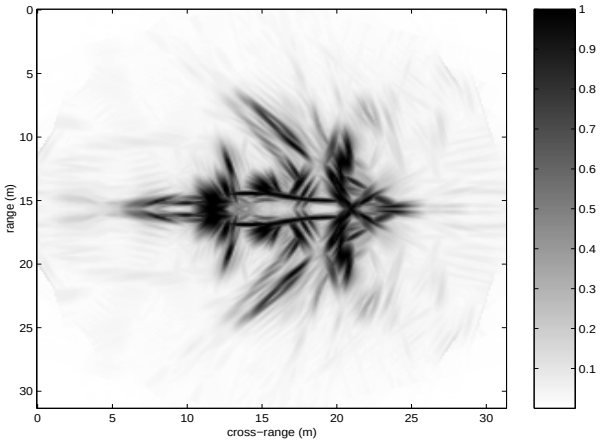

Fig. 9. Synthesized image by STFT from instantaneous images, 3^o wide hamming window used.

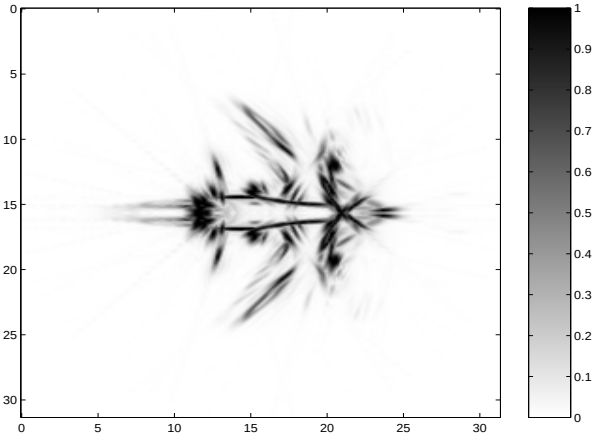

Fig. 10. Synthesized image by SPWVD from instantaneous images.